Pergamon

Geochimica et Cosmochimica Acta, Vol. 66, No. 13, pp. 2421–2438, 2002

0016-7037/02 $22.00 + .00

PII S0016-7037(02)00849-9

Solubility behavior of alkaline earth and alkali aluminosilicate components in aqueous fluids in the Earth's upper mantle

BJORN O. MYSEN*

Geophysical Laboratory, Carnegie Institution of Washington, 5251 Broad Branch Rd., N.W., Washington, DC 20015, USA

(*Received August* 8, 2001; *accepted in revised form January* 14, 2002)

Abstract—The solubility of aluminosilicate components in aqueous fluids in the 1200 to 1400°C and 0.8 to 2.0 GPa temperature- and pressure-range, respectively, has been determined for three compositions on the join $CaSi_4O_9$-$Ca(Ca_{0.5}Al)_4O_9$ with 0, 3, and 6 mol % Al_2O_3. The aluminosilicate solubility, X_{sil}, ranges from 0.5 to 4.2 mol %. Its temperature dependence is linear and ranges between 0.7 and $4.2 \cdot 10^{-3}$ mol %/°C depending on pressure. The pressure-dependence of X_{sil} is also positive but nonlinear. The solubility decreases with increasing Al_2O_3 content.

The solubility was fitted to the expression:

$$X_{sil}(\text{mol \%}) = -2.6 \pm 0.7 - 0.20 \pm 0.02 \cdot X_{Al_2O_3}(\text{mol \%}) + 0.002 \pm 0.001 \cdot T(°C)$$
$$+ 0.86 \pm 0.04 \cdot P^2(\text{GPa}) \qquad R^2 = 0.96$$

This relationship is qualitatively similar to that of equivalent compositions in the Na_2O-Al_2O_3-SiO_2-H_2O system ($2Na^+$ is exchanged for $1Ca^{2+}$). However, in the latter system, the solubility is 2 to 3 times greater. The magnitude of the pressure, temperature, and composition effects in the latter system is also greater. The partial molar volume of H_2O in the Ca silicate–saturated aqueous fluids, $\bar{V}^{fluid}_{H_2O}$, ranges between ~17 and ~27 cm^3/mol depending on pressure, temperature, and compositions so that,

$$\bar{V}^{fluid}_{H_2O} = 20.1 \pm 0.7 - 0.0019 \pm 0.015 X_{Al_2O_3} + 7.0 \pm 0.5 \cdot 10^{-4} T(°C) - 6.97 \pm 0.08P, \quad R^2 = 0.995$$

where T is in K, P in GPa, and $X_{Al_2O_3}$ in mol %. The molar volume of silicate-saturated aqueous fluid is nearly identical to $\bar{V}^{fluid}_{H_2O}$ because H_2O is the dominant component.

The isochors of Ca-aluminosilicate-saturated aqueous fluids differ from those of pure H_2O. The pressure difference at given temperature ranges between 5 and 10% in the 0.8 to 2.0 GPa and 1000 to 1400°C pressure- and temperature-range. For comparison, in the Na_2O-Al_2O_3-SiO_2-H_2O system this difference is between 5 and 30% depending primarily on fluid density and pressure. This difference between the Na- and Ca-system reflects the different solubility of Ca- and Na-silicate in aqueous fluids. *Copyright © 2002 Elsevier Science Ltd*

1. INTRODUCTION

Aqueous fluids are important materials transport agents in the Earth's crust and upper mantle. This is particularly so near convergent plate boundaries where there is evidence for elevated H_2O contents. This evidence includes glass in volcanic rocks, inclusions in phenocrysts in island arc volcanics, and results from laboratory experiments. All these lines of evidence commonly indicate H_2O contents on the order of 5 wt.% of island arc magmas at the time of eruption and perhaps 1 to 3 wt.% in the magma in its upper mantle source region (Sakuyama, 1979; Skirius et al., 1990; Schiano et al., 1995; Gerlach et al., 1996; Rutherford and Devine, 1996; Sobolev and Chaussidon, 1996). Results of experimental partial melting studies are also consistent with high H_2O activity during magma formation in the upper mantle beneath island arcs (Eggler, 1972; Kushiro, 1972, 1990; Merzbacher and Eggler, 1984; Gaetani et al., 1993).

The source of this H_2O most likely is subducted oceanic lithosphere from which H_2O is released by dehydration of hydrous minerals. This H_2O may equilibrate with the residual slab material and carry chemical signatures of the descending slab into the overlying mantle wedge. Signatures of slab components in volcanic rocks in island arcs have been detected in their trace element and isotope geochemistry (Bebout et al., 1993; Shibata and Nakamura, 1997; Heath et al., 1998). Slab signatures can also be observed in the trace element geochemistry of mantle-derived xenoliths in island arcs (Maury et al., 1992; Ionov and Hofmann, 1995). Evidence for major element metasomatism that involves silica, alkali, and alkaline earth enrichments in the peridotite wedge above subducting slabs is available in the form orthopyroxene overgrowth on olivine, and by the presence of pargasite and occasionally phlogopite in ultramafic xenoliths in volcanic rocks from arc settings (Riter and Smith, 1996; Aoki, 1987; Swanson et al., 1987).

To describe the interaction processes between melts, minerals, and aqueous fluids in the pressure and temperature regime of the upper mantle, experimental characterization of the solubility behavior of silicate components in aqueous fluids as a function of pressure, temperature, and bulk chemical composition is needed. Recent experimental data from the system MgO-SiO_2-H_2O indicate that at 1 to 2 GPa pressure several mol% silica can be dissolved in aqueous fluid (Zhang and Frantz, 2000). This solubility increases to tens of mol% at higher

* (mysen@gl.ciw.edu).

Table 1. Electron microprobe analyses of the starting materials.[a]

	CS4	CS4A3	CS4A6
SiO_2	80.12	76.69	75.49
Al_2O_3	0.28	4.68	9.29
CaO	19.60	18.63	15.25

[a]See text for discussion of sample preparation and analyses.

pressure (Fujii et al., 1996; Stalder et al., 2001). In peralkaline portions of the systems K_2O-Al_2O_3-SiO_2-H_2O and Na_2O-Al_2O_3-SiO_2-H_2O in 0.8 to 2.0 GPa pressure- and 700 to 1300°C temperature-range alkali aluminosilicate solubility in aqueous fluids is 1 to 10 mol% depending on pressure, temperature, and bulk composition (Mysen and Acton, 1999; Mysen and Wheeler, 2000). In meta-aluminous systems such as $NaAlSi_3O_8$-H_2O and $NaAlSiO_4$-H_2O the solubility in aqueous fluids may be even higher, perhaps to the point of complete miscibility between aqueous fluid and hydrous silicate melt (Shen and Keppler, 1995; Bureau and Keppler, 1999; Stalder et al., 2000).

The available experimental data on alkali aluminosilicate solubility in aqueous fluids cannot, however, be used directly to describe more complex natural systems without knowledge of the role of other metals such as alkaline earths. It is the purpose of this report, therefore, to address a broader compositional range by determination of the solubility behavior of Ca-aluminosilicate components in the system CaO-Al_2O_3-SiO_2-H_2O and to compare this behavior with solubility data available for compositions in the systems K_2O-Al_2O_3-SiO_2-H_2O and Na_2O-Al_2O_3-SiO_2-H_2O.

2. EXPERIMENTAL METHODS

Starting compositions were along the join $CaSi_4O_9$ - $Ca(Ca_{0.5}Al)_4O_9$. Three compositions, denoted CS4 (0 mol % Al_2O_3), CS4A3 (3 mol % Al_2O_3), and CS4A6 (6 mol % Al_2O_3), were used. These compositions were chosen so that on a molar basis, they have Al_2O_3 and SiO_2 concentrations similar to compositions KS4, KS4A3, KS4A6, NS4, NS4A3, and NS4A6 employed in the systems K_2O-Al_2O_3-SiO_2-H_2O and Na_2O-Al_2O_3-SiO_2-H_2O by Mysen and Acton (1999) and Mysen and Wheeler (2000). Instead of alkalis an equivalent proportion of Ca was used (1Ca = 2Na = 2K). In this manner we may compare directly the effect of metal cation type on the solubility.

Anhydrous starting materials were made from mixtures of spectroscopically pure $CaCO_3$, Al_2O_3, and SiO_2 ground under alcohol for ~1 h, decarbonated during slow heating (~1.5°C/min), heated at 1650°C at 0.1 MPa for 60 min, and then quenched. After this process, starting materials CS4 and CS4A3 consist of a mixture of a silica polymorph and glass, whereas CS4A6 was a glass. The starting materials were crushed to $\geq$20 μm grain size and stored at 110°C when not in use. To make these materials amenable to electron microprobe analyses to ascertain their composition, a portion of each starting composition was mixed with $LiBO_2$ with $LiBO_2$:silicate = 4:1, melted, and quenched to glass. Electron microprobe analyses, obtained with a JEOL model 8900 with 15 kV accelerating voltage and 10 nAmp beam current, recalculated to 100% silicate, are shown in Table 1.

High-pressure and high-temperature experiments were conducted in the solid-media, high-pressure apparatus (Boyd and England, 1960). The starting materials (0.3–4.0 mg) were loaded together with double-distilled, deionized H_2O (10–35 μL depending on desired H_2O content) into 3-mm O.D. Pt containers. Water was loaded with a microsyringe with 0.1 μL precision. The exact amount of H_2O added was determined from the weight of H_2O. The weighing accuracy for both silicate starting material and H_2O is $\pm$0.02 mg. The Pt containers were welded shut while submerged in liquid N_2 and subjected to experimental conditions in 19-mm-diameter furnace assemblies (Kushiro, 1976). Temperatures were measured with Pt-Pt90Rh10 thermocouples with no correction for pressure on their electromotoric force (emf). Although the exact effect of pressure on the emf depends on the details of the high-pressure furnace assemblies used, available data indicate that this effect is less than 10°C in the pressure-temperature range of the present experiments (Getting and Kennedy, 1970; Mao et al., 1971). The temperature uncertainty is, therefore, conservatively considered to be $\pm$10°C. Pressure was calibrated against the melting point of NaCl and the calcite-aragonite transformation (Bohlen, 1984). The pressure uncertainty thus obtained is $\pm$1 GPa.

The silicate-saturated aqueous fluids could not be quenched to a homogeneous fluid with the ~100°C/s quenching rate in the present experimental configuration. Instead, the quenched fluid was a mixture of crystalline Ca-silicate and silicate-rich bubbles (Fig. 1A). Raman spectra of this quench material, obtained with a confocal Dilor XY microRaman spectrometer (Mysen and Frantz, 1993), testifies to the silica-rich and amorphous nature of the quenched material in the bubbles (Fig. 2). The Raman spectra of the crystallized quench material (Fig. 1A) are consistent with a meta-silicate, thus leading to the suggestion that the crystalline quench phase may be wollastonite (Fig. 2). Compositions containing both H_2O-saturated silicate melt and silicate-saturated fluid quench to a glass with numerous inclusions of bubbles (Fig. 1B).

The composition of residual aqueous fluid at ambient pressure and temperature after precipitation of hydrous amorphous silicate and crystalline Ca-silicate during quenching does not, therefore, represent the composition of the fluid during an experiment. Chemical analysis of quenched fluids could not be used to determine the silicate solubility in these fluids and high pressure and temperature. Instead, phase equilibrium measurements that rely on optical examination (using a petrographic microscope at ~500$\times$ magnification) of the run products was employed to determine whether a specific composition contained fluid only or melt + fluid, (e.g., Figs. 1 and 3). The boundary between the fields of fluid only and fluid + melt defines the silicate solubility in aqueous fluid (Figs. 3A–C). The uncertainty in this silicate solubility, equal to the half-width of the experimental brackets, typically is $\pm$0.2 to 0.6 wt.%. Experiments were conducted at 0.8, 1.3, 1.65, and 2.0 GPa at 1200°, 1300°, and 1400°C to determine the solubility as a function of silicate composition, pressure, and temperature.

3. RESULTS

The Ca-silicate solubility in aqueous fluids as a function of pressure, temperature, and Al_2O_3 is shown in Figs. 4–6 with a summary least-squares fits of temperature, pressure, and composition relations to solubility in Table 2. In this report, the term "silicate" denotes bulk solubility of silicate in aqueous fluids whether or not the system contains aluminum. Also shown for comparison in Figures 4–6 (open symbols in inserts) are data for the equivalent Na-aluminosilicate compositions (from Mysen and Wheeler, 2000).

Throughout this report solubilities are given in terms of composition of the starting materials. Possible incongruent solubility behavior of silicate components in aqueous fluid noted, for example, in the system Na_2O-Al_2O_3-SiO_2-H_2O (Stalder et al., 2000; Mysen and Armstrong, 2002), would imply that the stoichiometry of dissolved silicate components in the fluids is not the same as that of the starting compositions. Whether or not this is the case in the present CaO-Al_2O_3-SiO_2-H_2O system is not known.

The Ca-silicate solubility is a positive and nonlinear function of pressure (Fig. 4; Table 2). Positive pressure-dependence of silicate solubility in aqueous fluids is in qualitative accord with results for other compositions such as SiO_2 (Manning, 1994), $NaAlSi_3O_8$ (Davis, 1972; Stalder et al., 1998), $KAlSi_3O_8$ (Morey and Hesselgesser, 1951), and MgO-SiO_2 (Fujii et al., 1996; Stalder et al., 2001).

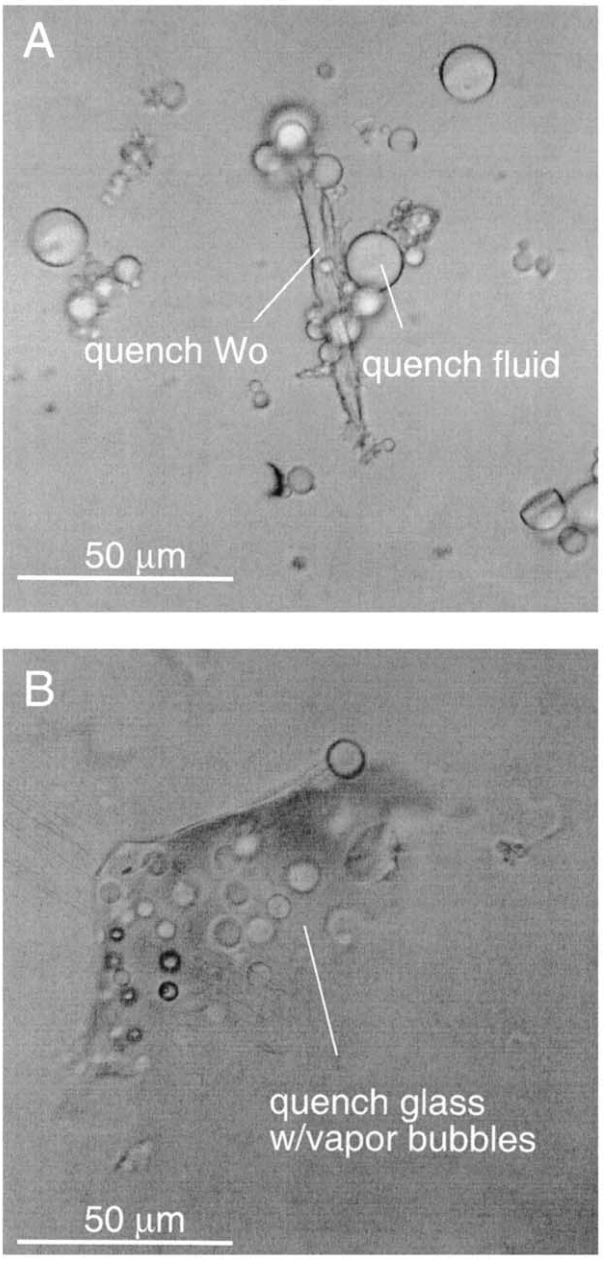

Fig. 1. Photomicrographs of typical experimental charges along the melt + fluid/fluid boundary. Both charges are from composition CS4A3. (A) Experimental charges from within the fluid-only stability field at 1.65 GPa and 1400°C and with 4.5 wt.% CS4A3 and 95.5 wt.% H_2O in starting material. (B) Within the fluid + melt stability field at 1.3 GPa and 1200°C and with 1.5 wt.% CS4A3 and 98.5 wt.% H_2O.

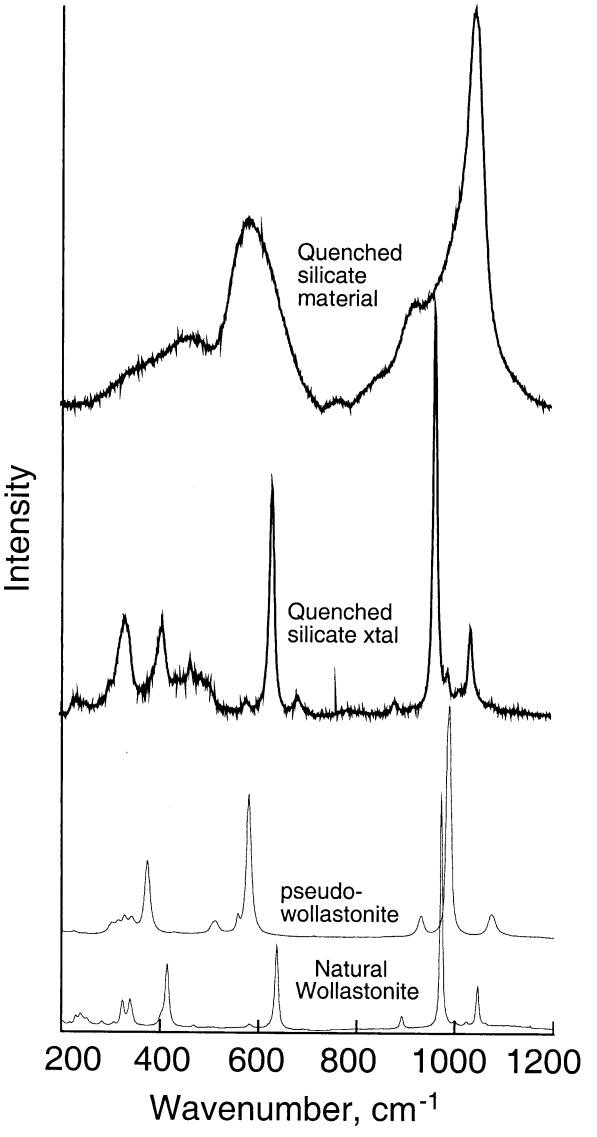

Fig. 2. Unpolarized Raman spectra of experimental charges compared with Raman spectra of wollastonite and pseudowollastonite. "Quenched silicate material"—Raman spectrum of quenched silicate material inside quench bubble from composition CS4 at 2.0 GPa and 1300°C with 5.4 wt.% CS4 and 93.6 wt.% H_2O in starting material. "Quenched silicate xtal"—Raman spectrum of quench silicate crystals from composition CS4 at 2.0 GPa and 1300°C with 5.4 wt.% CS4 and 93.6 wt.% H_2O in starting material. Raman spectra of crystalline wollastonite and pseudowollastonite (Richet et al., 1998) are shown for comparison of spectrum of "quenched silicate xtal."

The Ca-silicate solubility is a linear and positive function of temperature (Fig. 5; Table 2). The temperature-dependence, $(\partial X_{sil}/\partial T)_P$, increases with increasing pressure (which also results in increasing solubility). This correlation between total aluminosilicate solubility and the magnitude of its temperature-dependence extends to the Na-aluminosilicate systems. (Fig. 5; see also Mysen and Wheeler, 2000).

Finally, the solubility of Ca-silicate decreases in a nonlinear manner with increasing Al_2O_3 of the system (Fig. 6; Table 2). A more pronounced, but also nonlinear and negative correlation between silicate solubility and Al_2O_3 abundance was observed in the equivalent Na- and K-aluminosilicate systems (Fig. 6; see also Mysen and Wheeler, 2000; Mysen and Acton, 1999). As a result, the difference in silicate solubility between the two systems diminishes as they become more aluminous (Table 3).

From stepwise regression of all the data in the Ca-aluminosilicate system in the 0.8 to 2.0 GPa pressure- and 1200 to 1400°C temperature-range, the solubility can be expressed as:

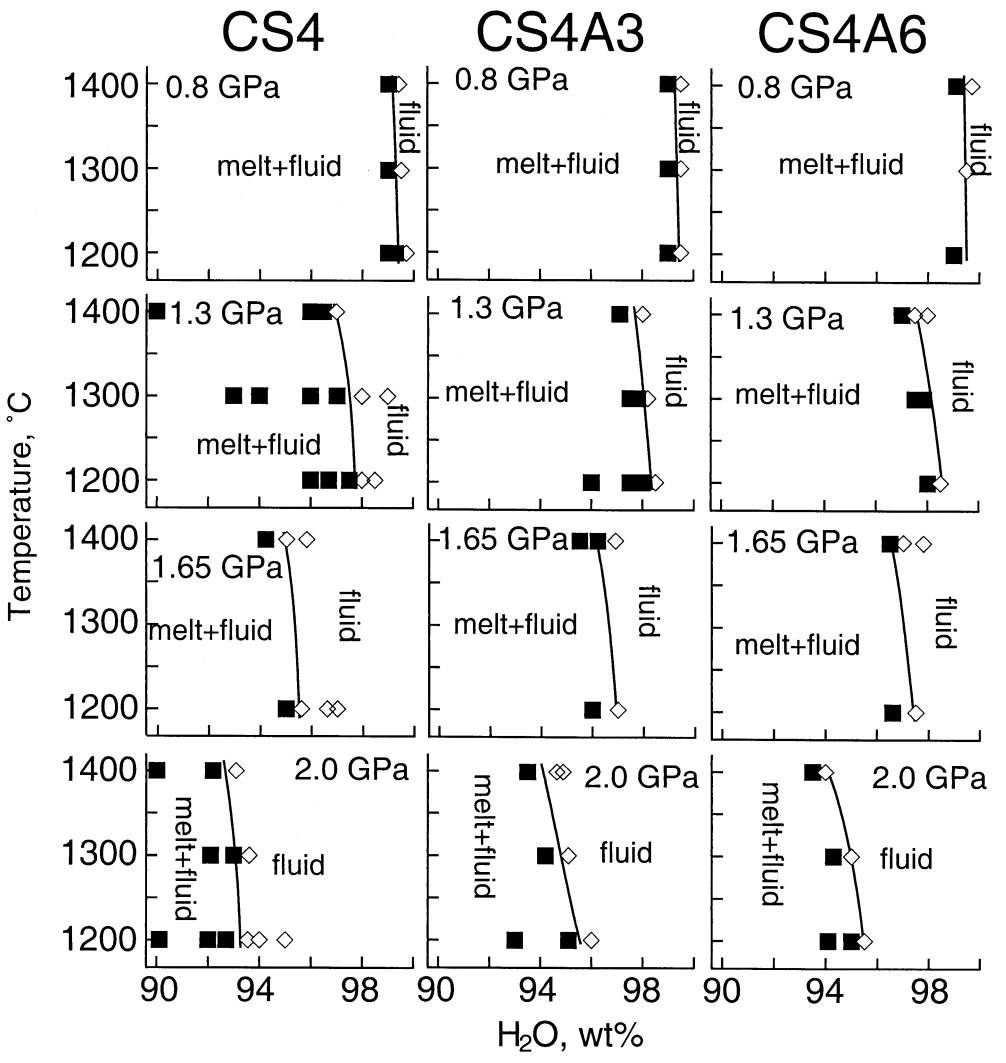

Fig. 3. Summary of experimental results. Phase boundaries obtained via third-order polynomial fit through the midpoints of the "fluid + melt" and "fluid" brackets.

$$X_{sil} = -2.6 \pm 0.7 - 0.20 \pm 0.02 \cdot X_{Al_2O_3} + 0.002 \pm 0.001 \cdot T + 0.86 \pm 0.04 \cdot P^2, \qquad R^2 = 0.96. \quad (1)$$

In Eqn. 1, X_{sil} and $X_{Al_2}O_3$ are in mol %, T in °C, and P in GPa.

In the stepwise regression, the procedure begins with an empty model and then adds independent variables in order of their ability to predict the dependent variable. The criterion for adding variables is the partial F-ratio. The latter ratio is the square of the value obtained from a *t*-test for the hypothesis that the coefficient of the variable in question equals zero.

From a similar regression of the silicate solubility for analogous compositions in aqueous fluids in the system Na_2O-Al_2O_3-SiO_2-H_2O, Mysen and Wheeler (2000) derived the expression:

$$X_{sil} = 1.3 \pm 3.5 - 1.3 \pm 0.9 \cdot X_{Al_2O_3} + 0.008 \pm 0.002 \cdot T + 13 \pm 4 \cdot P + 7.3 \pm 1.5 \cdot P^2, \qquad R^2 = 0.89. \quad (2)$$

The larger values of the regression coefficients in Eqn. 2 reflect the considerably higher solubility of the Na-aluminosilicate system as well as greater sensitivity of the solubility to alumina content, temperature, and pressure.

4. DISCUSSION

The silicate solubility in aqueous fluids may be used to estimate the influence of the dissolved silicate components on the partial molar volume of H_2O in the fluid. That information, in turn, can be used to estimate the effect of dissolved components on the density of silicate-saturated aqueous fluids in the temperature- and pressure-regime of the upper mantle of the earth.

4.1. Volume of H_2O in Silicate-saturated Solutions

Partial molar volume of H_2O in the fluids, $\bar{V}^{fluid}_{H_2O}$, can be extracted from the relationships:

$$\Delta G_T(P) = 0 = \Delta G_T\,(1bar) + RT\,ln\frac{a^{fluid}_{H_2O}}{f^{o}_{H_2O}} + \int_1^P \bar{V}^{fluid}_{H_2O}\,dP, \quad (3)$$

and,

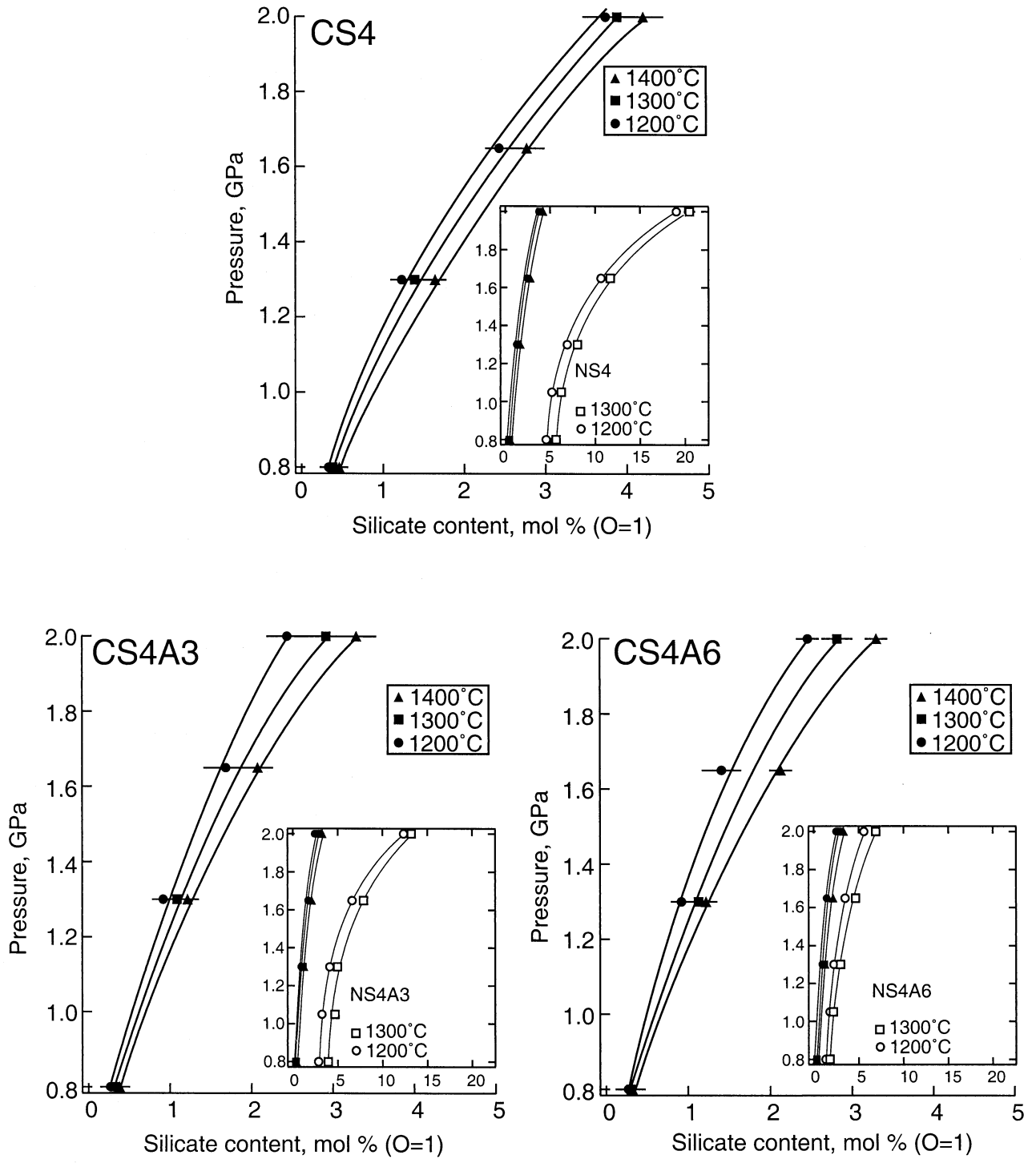

Fig. 4. Solubility of CS4, CS4A3, and CS4A6 composition in aqueous fluid as a function of pressure. Insets: Comparison of solubility with the solubility of equivalent compositions NS4, NS4A3, and NS4A6 in aqueous fluids as a function of pressure (data from Mysen and Wheeler, 2000). Mol % silicate solubility calculated on the basis of O = 1. See Table 2 for regression coefficients.

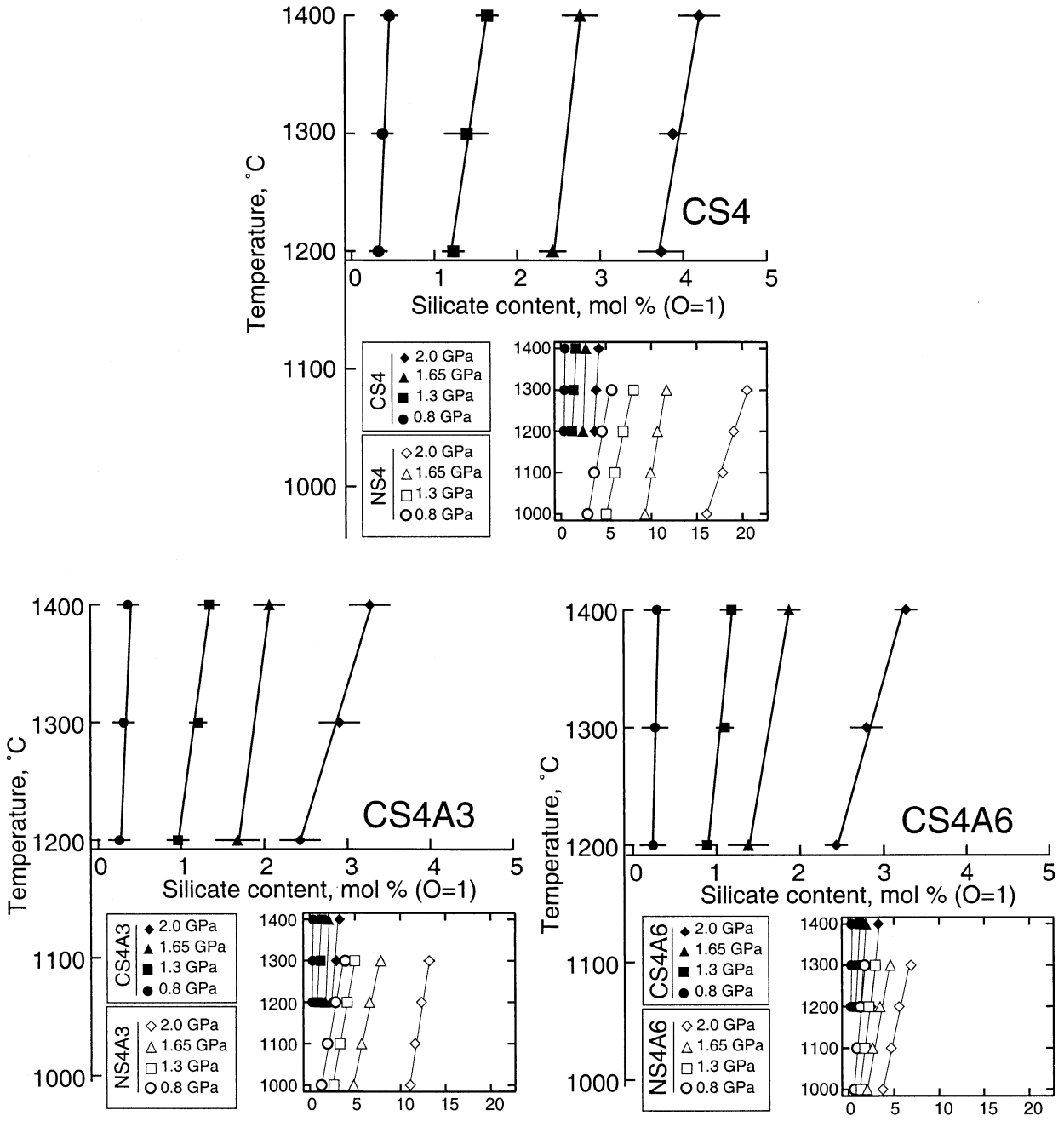

Fig. 5. Solubility of CS4, CS4A3, and CS4A6 composition in aqueous fluid as a function of temperature. Insets: Comparison of solubility with the solubility of equivalent compositions NS4, NS4A3, and NS4A6 in aqueous fluids as a function of pressure (data from Mysen and Wheeler, 2000). Mol % silicate solubility calculated on the basis of O = 1. See Table 2 for regression coefficients.

$$\Delta G_T(P) = 0 = \Delta G_T\,(1bar) + RT\left(\ln \gamma_{H_2O}^{fluid} + \ln \frac{X_{H_2O}^{fluid}}{f_{H_2O}^{o}}\right) + \int_1^P \bar{V}_{H_2O}^{fluid}\, dP, \quad (3a)$$

In Eqns. 3 and 3a, $a_{H_2O}^{fluid}$ is activity of H_2O in the fluid, $f_{H_2O}{}^{o}$ is the fugacity of pure H_2O (data from Haar et al., 1984, were used in the present calculations), and $\bar{V}_{H_2O}^{fluid}$ is the partial molar volume of H_2O in the fluid. The $X_{H_2O}^{fluid}$ and $\gamma_{H_2O}^{fluid}$ are the mol fraction and activity coefficient, respectively, of H_2O in the fluid. Provided that the activity coefficient of H_2O, $\gamma_{H_2O}^{fluid}$, does not vary over the pressure range of interest, the slope of the $(P\text{-}1)/RT$ vs. $\ln(f^{\circ}{}_{H_2O}/X_{H_2O}^{fluid})$ obtained from isothermal solubility data at several pressures equals $\bar{V}_{H_2O}^{fluid}$ at given temperature, T. The assumption that $\gamma_{H_2O}^{fluid}$ is constant cannot be tested

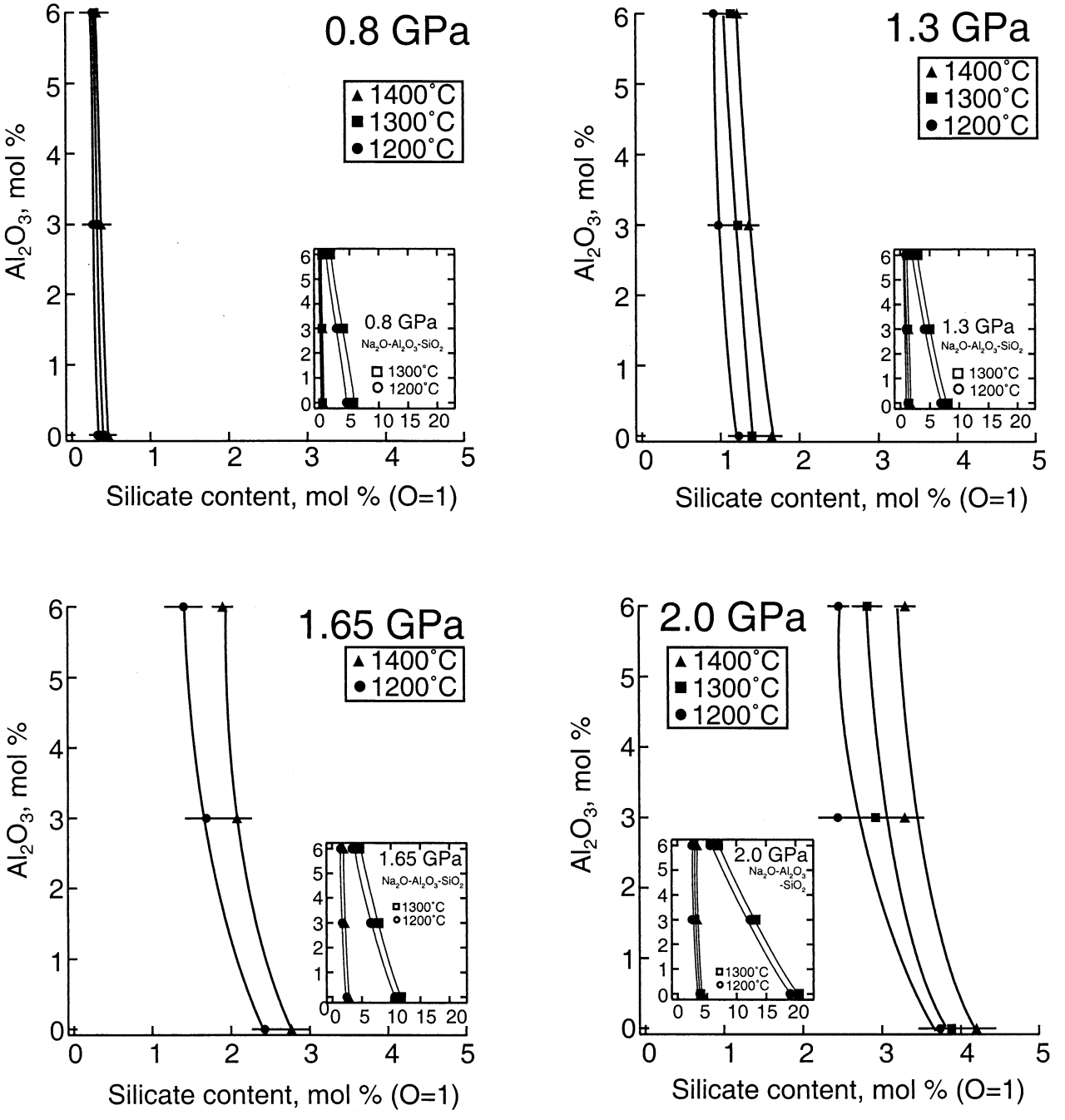

Fig. 6. Solubility of Ca-silicate in aqueous fluid as a function of Al_2O_3 content at pressures and temperatures indicated. Insets: Comparison of solubility with the solubility of equivalent compositions NS4, NS4A3, and NS4A6 in aqueous fluids as a function of pressure (data from Mysen and Wheeler, 2000). Mol % silicate solubility calculated on the basis of O = 1. See Table 2 for regression coefficients.

rigorously with available data for Ca silicate–saturated aqueous fluid. However, in the equivalent Na_2O-Al_2O_3-SiO_2-H_2O system in approximately the same temperature- and pressure-range (1000–1300°C; 0.8–2.0 GPa), partition coefficients for Na_2O, Al_2O, and SiO_2 between coexisting aqueous fluid and melt are linear functions of the oxide concentrations in the aqueous fluid (Mysen and Wheeler, 2001). That observation leads to the suggestion that the activity coefficients in the fluid of these three components and, therefore, of H_2O are constant. The aluminosilicate content of the aqueous fluids in the Na_2O-Al_2O_3-SiO_2-H_2O system (Mysen and Wheeler, 2000) is 2 to 3 times higher than in those in the present study of the CaO-Al_2O_3-SiO_2-H_2O system. It appears reasonable, therefore, to conclude that $\gamma_{H_2O}^{fluid}$ in Eqn. 3a also is constant in Ca silicate–saturated aqueous fluids in the pressure and temperature range under consideration. Equation (3a) can be used, therefore, to

Table 2. Temperature-, $(\partial X_{silicate}/\partial P)_P$, pressure-, $(\partial X_{silicate}/\partial P)_T$, and composition-dependence, $(\partial X_{silicate}/\partial X_{Al_2O_3})_{P,T}$ of silicate solubility in aqueous, aluminosilicate-saturated fluids.

	$(\partial X_{silicate}/\partial P)_T$ (mol %/GPa)		
Temp., °C	CS4	CS4A3	CS4A6
1200	$-0.9\ (0.8) + 1.3\ (0.3)\cdot P$	$0.1\ (0.6) + 0.60\ (0.2)\ )\cdot P$	$-1.0\ (1.1) + 0.9\ (0.4)\ )\cdot P$
1300[a]	$-9.7 + 1.3\cdot P$	$-0.3 + 0.9\cdot P$	$-0.3 + 0.6)\cdot P$
1400	$0.02\ (0.1) + 1.10\ (0.04)\ )\cdot P$	$-0.7\ (0.3) + 1.1\ (0.1)\cdot P$	$0.28\ (0.07) + 0.99\ (0.02)\cdot P$

	$(\partial X_{silicate}/\partial T)_P\cdot 10^3$ (mol %/°C)		
Pressure, GPA	CS4	CS4A3	CS4A6
0.8	0.68 (0.08)	0.541 (0.001)	0.2690 (0.0003)
1.3	2.1 (0.2)	1.9 (0.3)	1.4 (0.4)
1.65[a]	1.7	1.9	2.5
2.0	2.3 (0.5)	4.2 (0.3)	4.2 (0.3)

	$(\partial X_{silicate}/\partial X_{Al_2O_3})_{P,T}$ (mol %/mol % Al_2O_3)[a]			
Temp., °C	0.8 GPa	1.3 GPa	1.65 GPa	2.0 GPa
1200	$-0.03 + 0.003\cdot X_{Al_2O_3}$	$-0.12 + 0.01\cdot X_{Al_2O_3}$	$-0.21 + 0.02\cdot X_{Al_2O_3}$	$-0.64 + 0.072\cdot X_{Al_2O_3}$
1300	$-0.02 + 0.0015\cdot X_{Al_2O_3}$	$-0.07 + 0.005\cdot X_{Al_2O_3}$	—	$-0.46 + 0.048\cdot X_{Al_2O_3}$
1400	$-0.03 + 0.001\cdot X_{Al_2O_3}$	$-0.12 + 0.008\cdot X_{Al_2O_3}$	$-0.12 + 0.008\cdot X_{Al_2O_3}$	$-0.46 + 0.051\cdot X_{Al_2O_3}$

[a]Three data points, no error calculation.

extract partial molar volume, $\bar{V}^{fluid}_{H_2O}$, of H_2O in aqueous fluids in the CaO-Al_2O_3-SiO_2-H_2O system.

The $(P\text{-}1)/RT$ vs. $\ln(f°_{H_2O}/X^{fluid}_{H_2O})$ relationships show a slight but distinct curvature (Fig. 7; see Table 4 for regression coefficients to the third-order polynomial used to fit the data). This curvature reflects decreasing partial molar volume of H_2O in the aqueous fluids with increasing pressure $[(\partial \bar{V}^{fluid}_{H_2O}/\partial P)_T < 1]$ (Fig. 8). The $(\partial \bar{V}^{fluid}_{H_2O}/\partial P)_T$ is constant for each composition and temperature, and $(\partial^2 \bar{V}^{fluid}_{H_2O}/\partial T \partial P)$ is positive (Table 5) similar to the behavior of the equivalent compositions in the system Na_2O-Al_2O_3-SiO_2-H_2O (Mysen and Wheeler, 2000). The $(\partial \bar{V}^{fluid}_{H_2O}/\partial P)_T$ is independent of Al_2O_3 in the CaO-Al_2O_3-SiO_2-H_2O system (Table 5), whereas in the equivalent Na_2O-Al_2O_3-SiO_2-H_2O system, $(\partial \bar{V}^{fluid}_{H_2O}/\partial P)_T$ is positively correlated with Al_2O_3 (Table 5). The pressure-dependence of $\bar{V}^{fluid}_{H_2O}$ in both systems differs from that of the molar volume of pure H_2O, $V°_{H_2O}$, which decreases with increasing pressure in the same pressure and temperature range (Haar et al., 1984; Brodholt and Wood, 1993).

The thermal expansivity, $(\partial \bar{V}^{fluid}_{H_2O}/\partial T)_P$, is nearly constant for each composition, but decreases systematically with increasing pressure (Fig. 9; see also Table 6), resembling that observed in the Na_2O-Al_2O_3-SiO_2-H_2O system (Table 6; see also Mysen and Wheeler, 2000). The thermal expansivity of pure H_2O in this pressure-/temperature-regime is also nearly constant for each pressure and decreases with increasing pressure (Haar et

Table 3. Differences in silicate solubility in aqueous fluids in the systems CaO-Al_2O_3-SiO_2-H_2O and Na_2O-Al_2O_3-SiO_2-H_2O[a].

	1200°C					
Pressure GPa	Δ(NS4-CS4)[b] (mol %)	CS4/NS4[c] (%)	Δ(NS4A3-CS4A3) (mol %)	CS4A3/NS4A3 (%)	Δ(NS4A6-CS4A6) (mol %)	CS4A6/NS4A6 (%)
0.8	4.2 (0.3)	7 (2)	2.6 (0.2)	10 (5)	1.1 (0.3)	20 (12)
1.3	5.6 (0.3)	18 (2)	3.1 (0.2)	24 (3)	1.3 (0.3)	41 (7)
1.65	8.2 (0.3)	23 (2)	4.9 (0.4)	26 (4)	2.1 (0.3)	41 (7)
2.0	15.3 (0.4)	20 (2)	9.9 (0.4)	20 (2)	3.1 (0.3)	44 (3)
	1300°C					
Pressure GPa	Δ(NS4-CS4) (mol %)	CS4/NS4 (%)	Δ(NS4A3-CS4A3) (mol %)	CS4A3/NS4A3 (%)	Δ(NS4A6-CS4A6) (mol %)	CS4A6/NS4A6 (%)
0.8	5.2 (0.3)	7 (2)	3.6 (0.3)	8 (3)	1.5 (0.3)	17 (10)
1.3	6.6 (0.5)	17 (4)	3.8 (0.3)	25 (3)	1.8 (0.3)	38 (5)
1.65	—	—	—	—	—	—
2.0	16.6 (0.7)	19 (1)	10.3 (0.4)	22 (2)	4.1 (0.3)	41 (3)

[a]Solubility data for compositions NS4, NS4A3, and NS4A6 are from Mysen and Wheeler (2000).
[b]Solubility diffrence between equivalent compositions in the Na_2O-Al_2O_3-SiO_2-H_2O and CaO-Al_2O_3-SiO_2-H_2O systems respectively.
[c]Solubility of composition in the CaO-Al_2O_3-SiO_2-H_2O system relative to those in the Na_2O-Al_2O_3-SiO_2-H_2O (%).

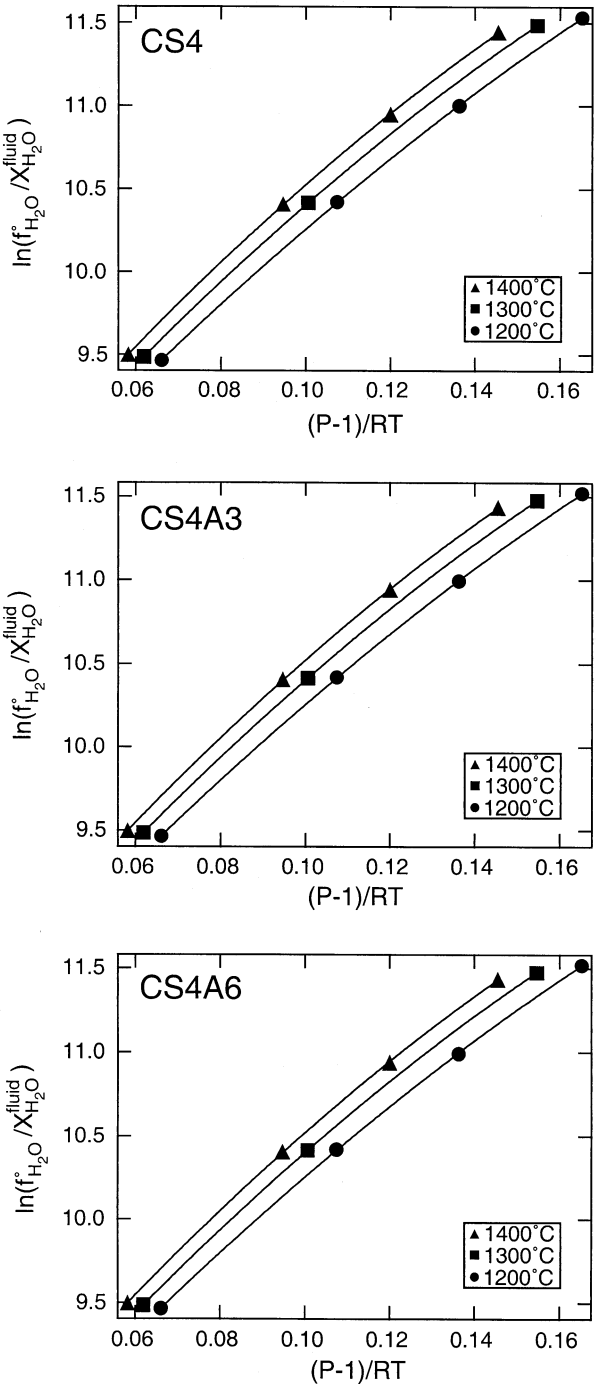

Fig. 7. Ln ($f^{o}_{H_2O}/X^{fluid}_{H_2O}$) versus ($P$-1)/$RT$ at the temperatures and for the compositions indicated. The size of symbols is greater than the uncertainty in the ln ($f^{o}_{H_2O}/X^{fluid}_{H_2O}$) function. The fugacity of pure H_2O is from Haar et al. (1984). See Table 4 for regression coefficients.

al., 1984; Brodholt and Wood, 1993) in a manner resembling that observed in the silicate-saturated aqueous fluids (Fig. 9; Table 6). The thermal expansion coefficients for pure H_2O, α_{H_2O}, are, however, slightly larger than that for the silicate-saturated aqueous fluid. This difference probably reflects the presence of significant dissolved silicate components, whose

Table 4. Coefficients for polynomial fit, ln ($f^{\circ}_{H_2O}/X^{fluid}_{H_2O}$) = a + b[($P$-1)/$RT$] + c[($P$-1)/$RT$]^2.

	CS4		
Temperature, °C	a	b	c
1200	7.68 ± 0.04	29.5 ± 0.7	−37.7 ± 2.9
1300[a]	7.71	31.5	−45.8
1400	7.78 ± 0.04	32.5 ± 0.9	−50.6 ± 4.3
		CS4A3	
	a	b	c
1200	7.67 ± 0.04	29.7 ± 0.7	−39.0 ± 3.2
1300[a]	7.71	31.7	−47.1
1400	7.78 ± 0.05	32.5 ± 1.0	−51.1 ± 4.9
		CS4A6	
	a	b	c
1200	7.68 ± 0.04	29.5 ± 0.9	−38.3 ± 4
1300[a]	7.71	31.6	−47.0
1400	7.78 ± 0.05	32.4 ± 1.0	−50.3 ± 5.3

[a]Only three pressure points at 1300°C. Hence, no uncertainty can be estimated.

thermal expansivity likely is considerably less than that of pure H_2O.

The temperature-, pressure-, and composition-dependence of the partial molar volume of H_2O in Ca-silicate saturated aqueous liquids (CAS) can be fitted via stepwise regression to a simple equation of the form:

$$\bar{V}^{fluid}_{H_2O}(CAS) = 20.1 \pm 0.7 - 0.019 \pm 0.015X_{Al_2O_3} + 7.0 \pm 0.5 \cdot 10^{-4}\,T(K) - 6.97 \pm 0.08P(GPa) \qquad R^2 = 0.995 \tag{4}$$

This fit compares with results for the partial molar volume of H_2O for the compositions in the equivalent Na_2O-Al_2O_3-SiO_2-H_2O (NAS) system (data from Mysen and Wheeler, 2000):

$$\bar{V}^{fluid}_{H_2O}(NAS) = 15.8 \pm 1.0 - 0.17 \pm 0.03X_{Al_2O_3} + 90 \pm 10 \cdot 10^{-4}T\,(K) - 4.4 \pm 0.02P\,(GPa) \qquad R^2 = 0.95 \tag{5}$$

The larger temperature and composition coefficients in the Na_2O-Al_2O_3-SiO_2-H_2O system reflect the much greater sensitivity of $\bar{V}^{fluid}_{H_2O}$ to composition and temperature in these latter fluids.

The bulk modulus,

$$G = \frac{1}{\beta} = \left(\frac{1}{-\frac{1}{V_o}\left(\frac{\partial \bar{V}^{fluid}_{H_2O}}{\partial P}\right)} \right), \tag{6}$$

for H_2O in Ca silicate–saturated aqueous fluids is constant and slightly above 4 GPa in the 0.8 to 2.0 GPa and 1200 to 1400°C pressure- and temperature-range, respectively (Table 6). In comparison, for the equivalent compositions in the Na_2O-Al_2O_3-SiO_2-H_2O system, the bulk modulus decreases with increasing Al_2O_3 although in this latter system, for each composition the bulk modulus remains constant (Mysen and Wheeler, 2000; Table 6). This behavior of the bulk modulus

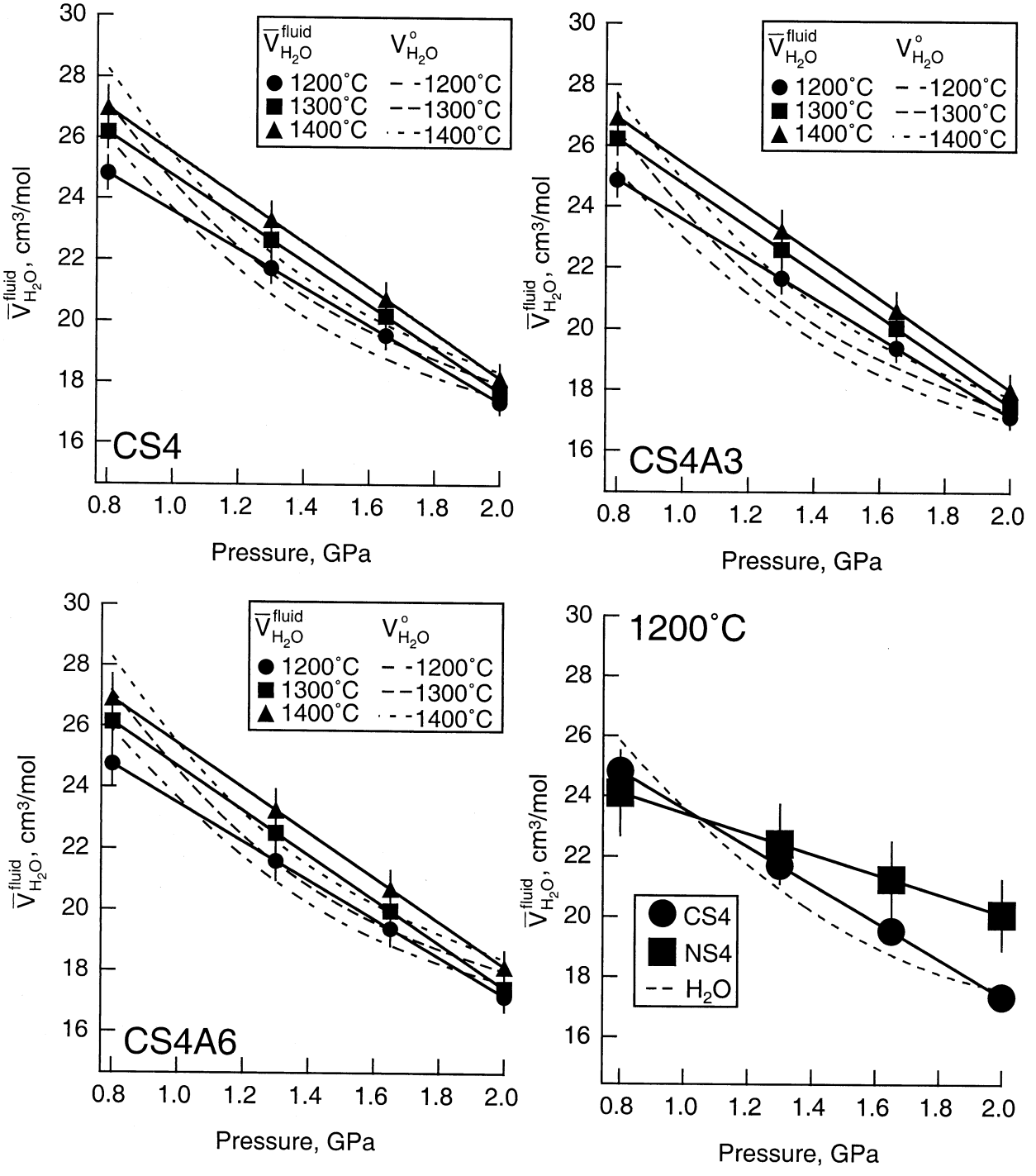

Fig. 8. Partial molar volume of H_2O, $\bar{V}^{fluid}_{H_2O}$, as a function of pressure for compositions indicated. The $\bar{V}^{fluid}_{H_2O}$ for composition NS4 is from Mysen and Wheeler (2000). Also shown is the molar volume of pure H_2O, $V^{o}_{H_2O}$, from Haar et al. (1984). See Table 5 for regression coefficients.

contrasts with that of the bulk modulus of pure H_2O, which decreases significantly with increasing pressure in the pressure-temperature regime of these experiments (Haar et al. 1984, see also dashed lines in Fig. 8). In other words, in both the CaO-Al_2O_3-SiO_2-H_2O and Na_2O-Al_2O_3-SiO_2-H_2O systems, H_2O in the silicate-saturated aqueous fluids is less compressible than pure H_2O at the lower pressures, and more compressible than pure H_2O at the higher pressures. Qualitatively similar behavior can be inferred from the aluminosilicate solubility in aqueous fluids in the K_2O-Al_2O_3-SiO_2-H_2O system (Mysen and Acton, 1999).

Table 5. Pressure dependence of partial molar volume[a] of H_2O) in aluminosilicate-saturated aqueous solutions.

	CS4		NS4[b]			
Temp., °C	a	b	a	b	a	b
1200	29.81 (0.05)	−6.23 (0.02)	26.60 (0.05)	−3.34 (0.03)		
1300	31.96 (0.05)	−7.09 (0.03)	27.51 (0.04)	−3.43 (0.03)		
1400	32.86 (0.03)	−7.36 (0.02)				
	CS4A3		NS4A3[b]		KS4A3[c]	
1200	30.02 (0.02)	−6.44 (0.06)	27.55 (0.04)	−4.43 (0.03)	29.39 (0.02)	−5.86 (0.01)
1300	32.10 (0.05)	−7.29 (0.03)	29.01 (0.05)	−5.00 (0.03)	31.03 (0.06)	−6.49 (0.04)
32.87 (0.07)	−7.43 (0.03)					
	CS4A6		NS4A6[b]			
1200	29.82 (0.06)	−6.33 (0.04)	29.3 (0.06)	−6.06 (0.04)		
1300	32.00 (0.01)	−7.73 (0.01)	30.83 (0.06)	−6.57 (0.03)		
1400	32.76 (0.08)	−7.32 (0.06)				

[a] $\bar{V}_{H_2O}^{fluid} = a + b \cdot P(GPa)$.
[b] From Mysen and Wheeler (2000).
[c] From Mysen and Acton (1999).

4.2. Density of Silicate-saturated Aqueous Solutions

Calcium silicate–saturated aqueous solutions in the pressure and temperature ranges under study dissolve up to nearly 20 wt.% silicate (depending on pressure, temperature, and bulk composition; see Fig. 3). This dissolved silicate may affect the solution density in part because the density of silicate components differs substantially from the density of pure H_2O and in part because $\bar{V}_{H_2O}^{fluid}$ (and its pressure- and temperature-derivatives) differs from the molar volume of pure H_2O, $V^{o}_{H_2O}$.

To calculate the molar volume and density of silicate-saturated aqueous fluids, partial molar volume silicate components and H_2O are needed. We will use the $\bar{V}_{H_2O}^{fluid}$ from the present results (Figs. 8 and 9). The partial molar volume of the oxides in solution may be approximated with those for oxides in silicate melts (Lange and Carmichael, 1987; Kress and Carmichael, 1991; Lange, 1997). This approximation is justified in light of current knowledge of the silicate speciation in silicate-saturated aqueous fluids in pressure-temperature ranges similar to those of the present experiments (Mysen, 1998; Zotov and Keppler, 2000). These species (or complexes) are associated and polymerized metal silicate complexes. Association of metal silicate solute in these aqueous fluids is likely because the dielectric constant of H_2O is quite low at high temperature such as those of the present experiments (Pitzer, 1983). Decreasing dielectric constant promotes association of the solute, which has been observed in various other salt solutes in aqueous fluids (Quist and Marshall, 1968; Frantz and Popp, 1981). We suggest, therefore, that in both hydrous silicate melts and silicate-saturated aqueous fluids at high pressure and temperature, the dominant silicate species or complexes are of Q^i(M) type where i denotes the number of bridging oxygen in the silicate ($i > 0$) and M is the associated metal cation (M = Ca or Na in the present discussion). In both hydrous melts and aqueous fluid, water exists as protonated SiO_4^{4-} [Q^o(H)], as M·OH complexes, and as molecular H_2O (Mysen, 1998; Zotov and Keppler, 2000). It is because of these structural similarities between hydrous silicate melts and silicate-saturated aqueous fluid at high pressure and temperature that we suggest that the partial molar volume of oxides in the silicate-saturated aqueous fluid can be approximated with the values determined for silicate melts. Their concentration in aqueous fluids, however, is considerably lower than in the melts. We assume, however, that the partial molar volume of the oxides in the melts and the fluids does not depend on their concentration in the concentration range under consideration.

The molar volume of Ca silicate–saturated aqueous fluids is shown as a function of pressure in Figure 10. Also shown is a comparison between the molar volume of the equivalent compositions H_2O + CS4 and H_2O + NS4 at 1200°C. The partial molar volume of H_2O, $\bar{V}_{H_2O}^{fluid}$, in the NS4- and CS4-saturated aqueous fluids is also shown in Figure 10 together with the molar volume of pure H_2O, $V^{o}_{H_2O}$. The 1200°C temperature was used to illustrate the difference between its molar volume, V^{fluid}, and $\bar{V}_{H_2O}^{fluid}$ because among the compositions studied, the two compositions, CS4 and NS4, at this temperature exhibit the largest difference between V^{fluid} and $\bar{V}_{H_2O}^{fluid}$.

The molar volume of the silicate-saturated aqueous fluids is nearly identical to the partial molar volume of H_2O in the same fluid. This observation is a direct consequence of the relatively low silicate solubility in the fluid. The difference between V^{fluid} and $\bar{V}_{H_2O}^{fluid}$ is slightly larger in the Na_2O-Al_2O_3-SiO_2-H_2O system (Fig. 10; see also Mysen and Wheeler, 2000) in part because of the significantly greater solubility of Na-silicate components in those fluids.

We may, therefore, use $\bar{V}_{H_2O}^{fluid}$ as an approximation of V^{fluid} in Ca-silicate systems such as that studied here (as well as in Na-silicate systems; Mysen and Wheeler, 2000) at least in the pressure and temperature range under consideration.

The density of the silicate-saturated aqueous fluids, therefore, is:

$$\rho^{fluid} = \frac{M^{fluid}}{V^{fluid}} \sim \frac{M^{fluid}}{\bar{V}_{H_2O}^{fluid}}, \quad (7)$$

where M^{fluid} is the molecular weight of the silicate-saturated aqueous fluid.

The resulting pressure- and temperature-dependence of fluid density, ρ^{fluid}, governed by the composition-, pressure-, and temperature-dependence of $\bar{V}_{H_2O}^{fluid}$, and the molecular weight of

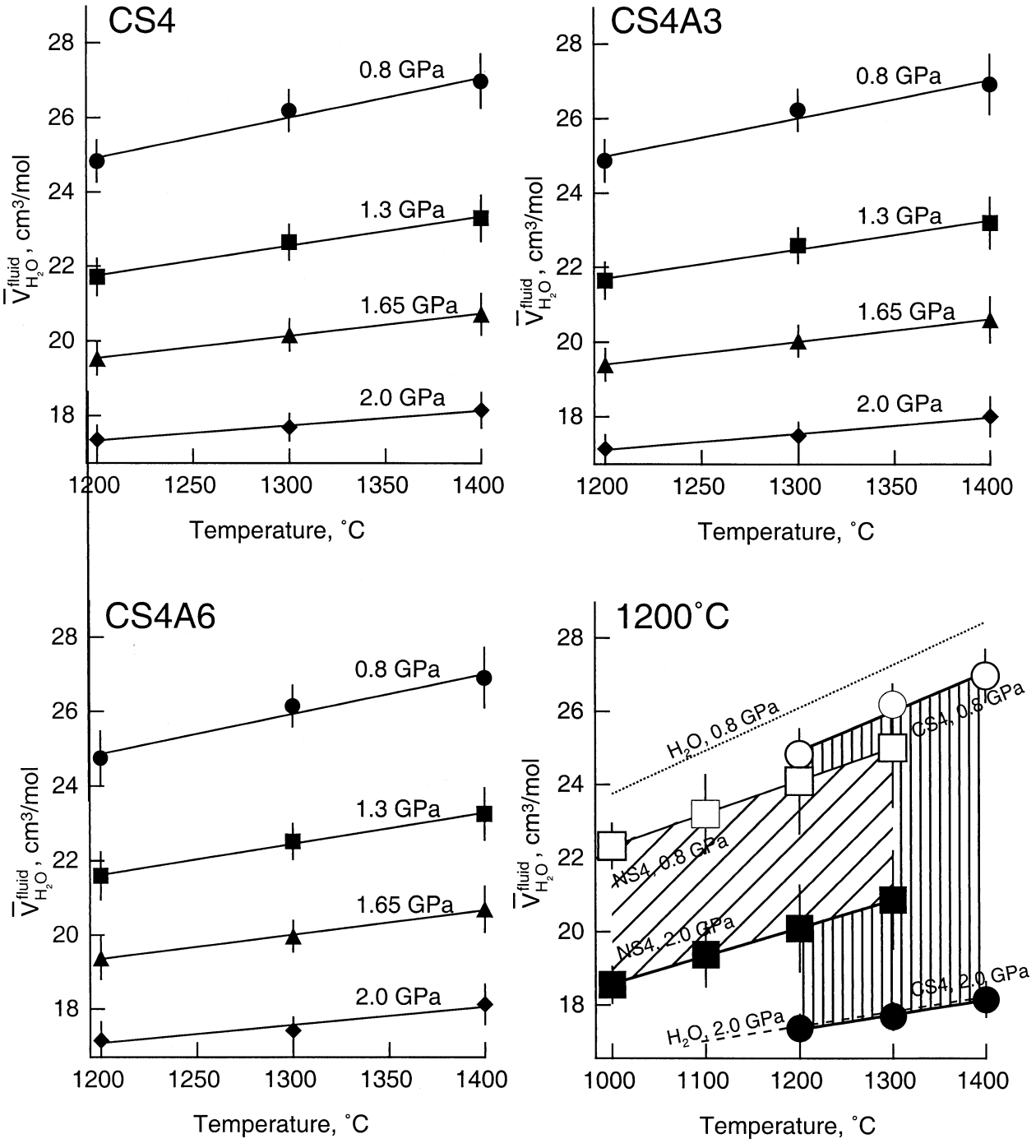

Fig. 9. Partial molar volume of H_2O, $\bar{V}^{fluid}_{H_2O}$, as a function of temperature for compositions indicated. The $\bar{V}^{fluid}_{H_2O}$ for composition NS4 is from Mysen and Wheeler (2000). Also shown is the molar volume of pure H_2O, $V^{o}_{H_2O}$, from Haar et al. (1984).

the fluid, is shown in Figure 11. The density of Al-free compositions, CS4 and NS4, as well as that of pure H_2O (Haar et al., 1984) is also compared in Fig. 11. The density of Ca silicate–saturated aqueous fluids is a nonlinear function of pressure. The $(\partial\rho^{fluid}/\partial P)_T$ increases with increasing pressure for all compositions (Fig. 11). The positive $(\partial\rho^{fluid}/\partial P)_T$ results from the strong positive and nonlinear dependence of solubility of silicate in the fluids with pressure (Fig. 4). This density behavior is qualitatively similar to that observed for Na silicate–saturated aqueous fluids (Mysen and Wheeler, 2000) in the same pressure and temperature range. The $(\partial\rho^{fluid}/\partial P)_T$ in the latter is system is, however, greater than for the Ca silicate–saturated aqueous fluids (see Fig. 11, for example) because of the larger silicate solubility, X_{sil}, and the larger $(\partial\bar{V}^{fluid}_{H_2O}/\partial P)_T$ in

Table 6. Compressibility, β,[a] bulk modulus, G,[b] and thermal expansion, α[c] of H_2O in aluminosilicate-saturated aqueous fluids.

	Compressibility, GPa^{-1}						
Temperature °C	CS4	NS4[d]	CS4A3	NS4A3	CS4A6	NS4A6	H_2O[e]
1200	0.209 (0.001)	0.126 (0.001)	0.214 (0.002)	0.161 (0.001)	0.212 (0.001)	0.206 (0.001)	0.49–0.22P
1300	0.223 (0.001)	0.124 (0.001)	0.227 (0.001)	0.172 (0.001)	0.227 (0.001)	0.213 (0.001)	0.51–0.22P
1400	0.224 (0.001)		0.226 (0.001)		0.223 (0.002)		0.52–0.24P
	Bulk modulus, GPa						
Temperature °C	CS4	NS4	CS4A3	NS4A3	CS4A6	NS4A6	
1200	4.78 (0.02)	7.90 (0.1)	4.66 (0.04)	6.21 (0.04)	4.71 (0.03)	4.85 (0.02)	
1300	4.49 (0.02)	8.01 (0.1)	4.40 (0.02)	5.81 (0.03)	4.40 (0.02)	4.69 (0.02)	
1400	4.46 (0.01)		4.42 (0.02)		4.48 (0.04)		
	Thermal expansion $\cdot 10^4$, K^{-1}						
Pressure GPa	CS4	NS4	CS4A3	NS4A3	CS4A6	NS4A6	H_2O
0.8	9.2 (1.8)	6.4 (2.3)	7.9 (2.3)	8.2 (0.3)	9.2 (2.5)	9.2 (0.2)	13.3
1.3	6.5 (0.9)	6.9 (0.1)	6.3 (1.0)	5.2 (0.1)	7.2 (0.6)	7.2 (0.2)	6.3
1.65	4.8 (0.2)	7.0 (0.2)	5.0 (0.6)	4.6 (0.2)	5.8 (0.4)	5.8 (0.1)	4.5
2	3.1 (0.3)	7.0 (0.2)	3.6 (0.5)	3.0 (0.2)	4.3 (0.6)	4.1 (0.2)	3.5

[a]Compressibility, $\beta = -\frac{1}{V^o}\left(\frac{\partial \bar{V}^{fluid}_{H_2O}}{\partial P}\right)_T$, GPa^{-1}

[b]Bulk modulus: $G = \frac{1}{\beta}$, GPa

[c]Thermal expansion, $\alpha = \frac{1}{V_o}\left(\frac{\partial \bar{V}^{fluid}_{H_2O}}{\partial T}\right)_P$, K^{-1}

[d]Based on solubility data from Mysen and Wheeler (2000).

[e]Data from Haar et al. (1984).

Na_2O-Al_2O_3-SiO_2-H_2O system compared with the CaO-Al_2O_3-SiO_2-H_2O system (Figs. 4 and 8). This behavior is in contrast to that of pure H_2O whose density decreases with increasing pressure (Haar et al., 1984; Brodholt and Wood, 1993).

The density difference between that of silicate-saturated aqueous fluids and pure H_2O passes through a minimum with increasing pressure (Fig. 12) because of the difference between $(\partial V^o_{H_2O}/\partial P)_T$ and $(\partial \bar{V}^{fluid}_{H_2O}/\partial P)_T$ (Fig. 8) and because the silicate solubility in aqueous fluids is significantly pressure-dependent (Fig. 4). Between ~1.1 and 1.7 GPa the density of pure H_2O exceeds that of the Ca silicate–saturated aqueous solutions. A qualitatively similar minimum occurs in the density difference between pure H_2O and Na silicate–saturated fluids (Fig. 12). The fluids in the latter system, however, remain more dense than pure H_2O at all pressures (Fig. 12) because of the considerably greater Na- than Ca-silicate solubility and the stronger pressure-dependence on the solubility in the Na system (Fig. 4).

From the pressure-, temperature-, and composition-dependent fluid density, stepwise regression yields the expression:

$$\log\rho^{fluid}(CAS) = -0.445 \pm 0.024 + 4 \pm 4\cdot 10^{-3}X_{Al_2O_3}(mol\%) + \frac{326 \pm 32}{T(^\circ C)}. \qquad R^2 = 0.993$$
$$+ 0.078 \pm 0.19P(GPa) + 0.027 \pm 0.007P^2 \quad (8)$$

From Eqn. 8 the P-T trajectory of isochors in this system is

$$P(GPa) = -1.444 + \frac{\sqrt{-326 + T(^\circ C)(0.523 + \log\rho^{fluid}(CAS) - 0.004X_{Al_2O_3}(mol\%)}}{\sqrt{T(^\circ C)}}. \quad (9)$$

From the Na-silicate solubility data from the equivalent Na_2O-Al_2O_3-SiO_2-H_2O system (data from Mysen and Wheeler, 2000), the respective relationships are:

$$\log\rho^{fluid}(NAS) = -0.282 \pm 0.0019 + 2 \pm 0.3\cdot 10^{-3}\cdot 10^{-3}X_{Al_2O_3}(mol\%), + \frac{220\pm 13}{T(^\circ C)}$$
$$+ 0.046 \pm 0.001P^2(GPa)\, R^2 = 0.991 \quad (10)$$

and,

$$P(GPa) = 4.6652 \sqrt{0.282 + \log\rho^{fluid}(NAS) - \frac{220}{T(^\circ C)} + 0.002X_{Al_2O_3}(mol\%)}. \quad (11)$$

A few isochors calculated from Eqns. 9 and 11 are shown in Figure 13. In Figure 13A, 0.8 and 1.0 g/cm^3 isochors were calculated for aqueous fluid saturated with the Al-free compositions, CS4 and NS4 (thick and thin solid lines, respectively). These isochors are compared with the 0.8 and 1.0 g/cm^3 isochors for pure H_2O (dashed lines; calculated with data from Haar et al., 1984).

The isochors of aqueous fluid saturated with either Ca- or

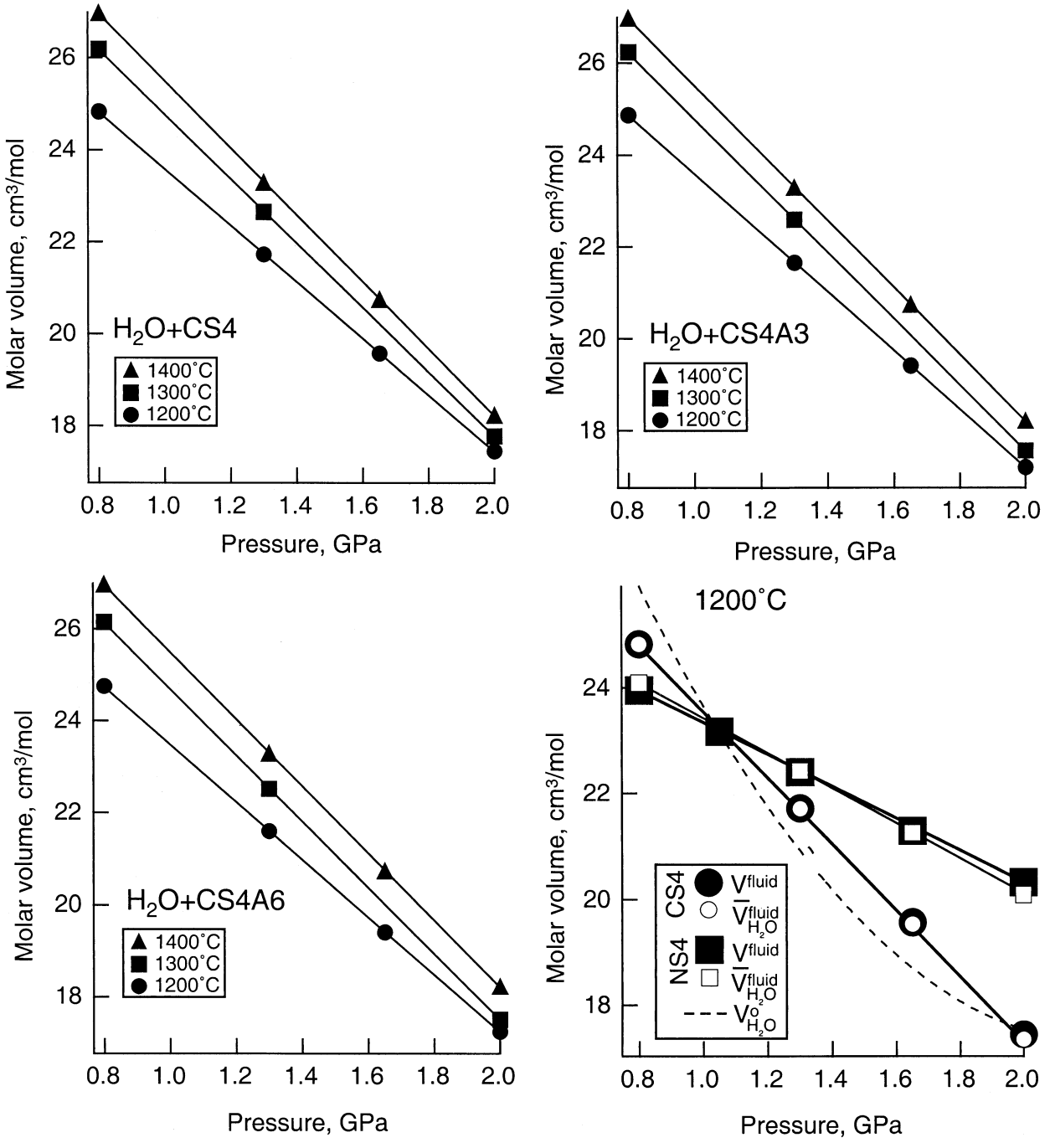

Fig. 10. Molar volume of H_2O as a function of pressure for compositions indicated. The molar volume for composition NS4 is from Mysen and Wheeler (2000). Also shown is the molar volume of pure H_2O, $V^o_{H_2O}$, from Haar et al. (1984).

Na-silicate differ significantly from those of pure H_2O (Fig. 13). At low densities ($\leq$0.9 g/cm^3), Ca silicate–saturated fluids are less dense than pure H_2O. This relationship is reversed at higher densities. Thus, for ρ_{fluid}(CAS) $\leq$ 0.9 g/cm^{-3} for given temperature and density, any pressure inferred from density based on the isochors of pure H_2O would underestimate pressure. At higher fluid densities, the reverse is true. In comparison, Na silicate–saturated fluids remain heavier than those of pure H_2O at any density. Thus, pressure estimates for Na silicate–saturated aqueous fluids from the density of pure H_2O would always lead to an overestimate.

The effect of Al_2O_3 on isochors of silicate-saturated fluids was estimated at 1000°C and 1400°C. By adding Al_2O_3 to the system, the silicate solubility decreases whether in the Ca- (Figs. 4 to 6), the Na-silicate system (Mysen and Wheeler, 2000), or the K-aluminosilicate system (Mysen and Acton, 1999). The effect of Al_2O_3 on solubility is greater in the Na- and K-aluminosilicate systems than in the Ca-aluminosilicate

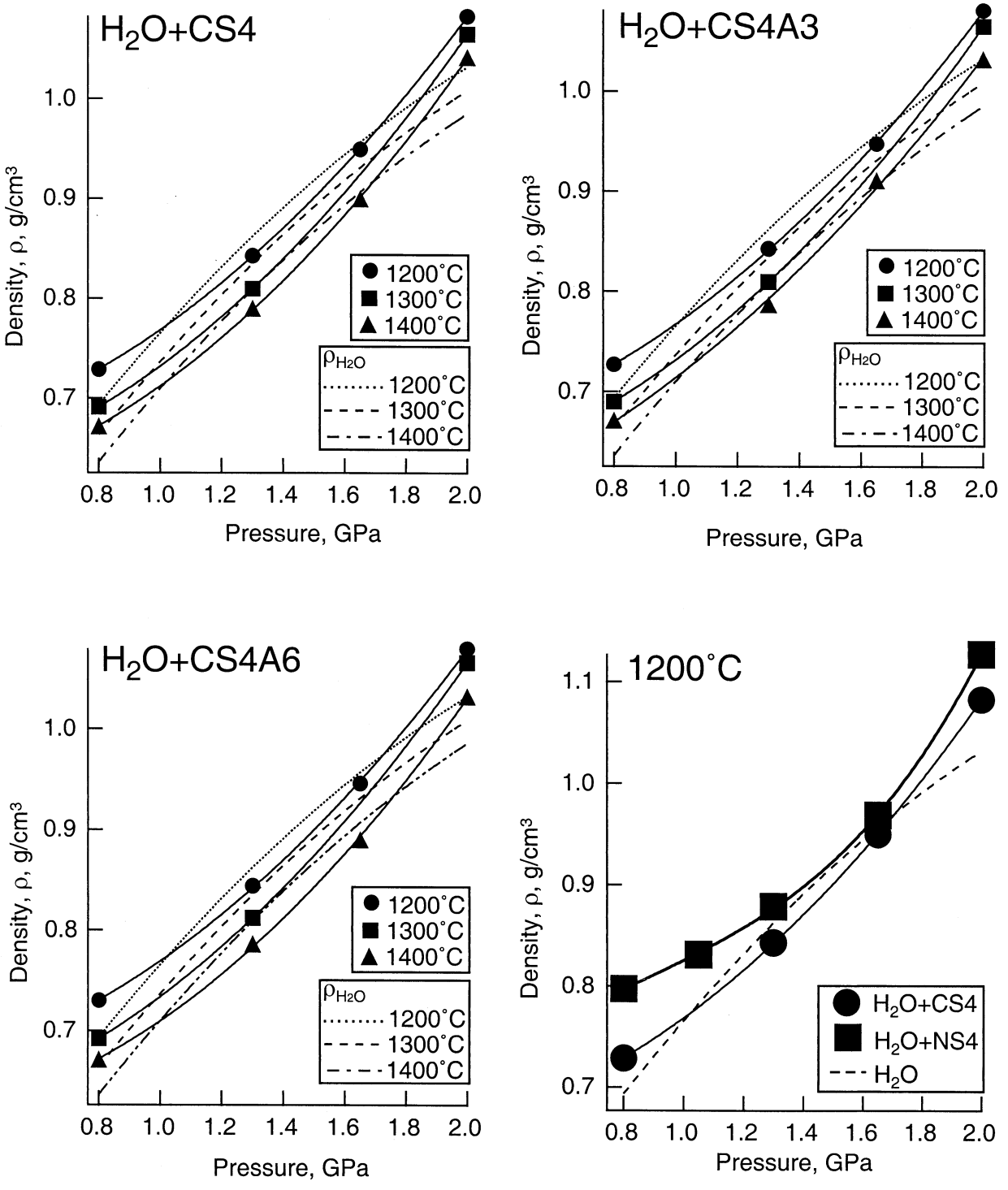

Fig. 11. Density of H_2O as a function of pressure for compositions indicated. The density of NS4 + H_2O fluid is from Mysen and Wheeler (2000). Also shown is the molar volume of pure H_2O, $V^o_{H_2O}$, from Haar et al. (1984). See text for detailed discussion of density calculations.

system. Therefore, at constant temperature and fluid density, the density difference between Na- (and K-, not shown) and Ca-saturated aqueous fluids decreases with increasing Al_2O_3 (Fig. 13).

The difference in P/T trajectory of the isochors in the Na_2O-Al_2O_3-SiO_2-H_2O and CaO-Al_2O_3-SiO_2-H_2O systems also changes with temperature because the temperature dependence of the silicate solubility in aqueous fluids in the two systems differs (Figs. 5 and 13). For fluid density less than ~0.85 g/cm^3, the pressure difference decreases in the temperature

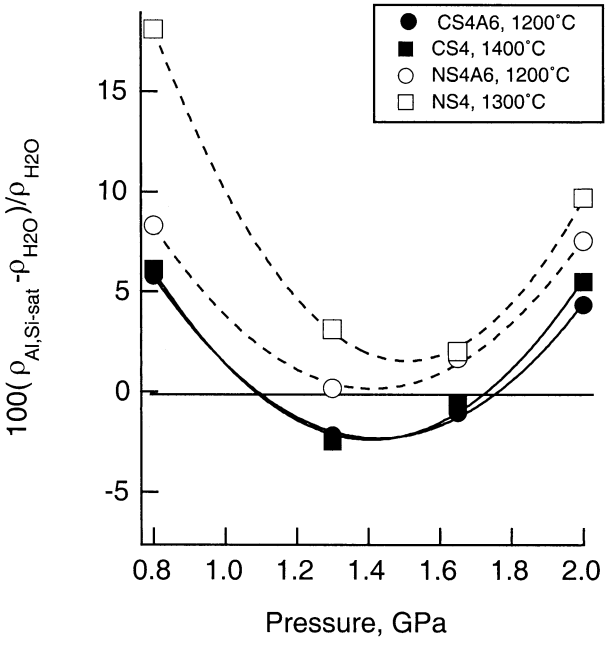

Fig. 12. Density difference between Na- and Ca-aluminosilicate-saturated aqueous relative to that of pure H_2O, $100(\rho_{Al,Si,-sat}-\rho_{H_2O})/\rho_{H_2O}$, for compositions indicated. The data for compositions, NS4 and NS4A6, are based on the solubility data of Mysen and Wheeler (2000).

interval between 1000° and 1400°C although the rate of decrease diminishes with increasing temperatures. For heavier fluids, the density difference between the two fluids increases with increasing temperature (Fig. 13). This behavior reflects the observation that the positive temperature-dependence of silicate solubility in the Na_2O-Al_2O_3-SiO_2-H_2O system is greater than that in the CaO-Al_2O_3-SiO_2-H_2O system (Fig. 5).

5. CONCLUDING REMARKS

The solubility of Ca-aluminosilicate components in aqueous fluids in the system CaO-Al_2O_3-SiO_2-H_2O ranges from <1 mol % to ~4 mol % in the 1200 to 1400°C temperature, and 0.8 to 2.0 GPa pressure range, respectively. The solubility is a positive function of both pressure and temperature and a negative function of Al_2O_3 content.

The solubility in the CaO-Al_2O_3-SiO_2-H_2O system is ~7–44% of that of equivalent compositions in the Na_2O-Al_2O_3-SiO_2-H_2O system. This solubility difference becomes smaller the higher the Al_2O_3 content.

Partial molar volume of H_2O in Ca silicate–saturated aqueous fluids, derived from the solubility data, ranges between 27 and ~17 cm^3/mol, and decreases as linear functions of pressure and increases as a linear function of temperature. Compared with H_2O in Na silicate–saturated fluids in the same pressure and temperature range, the $\bar{V}^{fluid}_{H_2O}$ in the Ca-silicate system is slightly higher in the low-pressure portion of the experimental pressure range and ≥2 cm^3/mol lower near 2 GPa. This difference in behavior is because the compressibility of Na silicate–saturated fluids is less than that of Ca silicate–saturated fluids.

The density of silicate-saturated aqueous fluids, whether with Na or Ca, increases with increasing pressure. The $(\rho^{fluid}_{H_2O}/\partial P)_T$ is positive in contrast to that of pure H_2O, where $(\rho^{fluid}_{H_2O}/\partial P)_T$ is negative. This difference results from the increasing solubility of aluminosilicate components with increasing pressure. As a result of these differences, isochors of aluminosilicate-saturated aqueous fluids differ from those of pure H_2O (Gerlach et al., 1996).

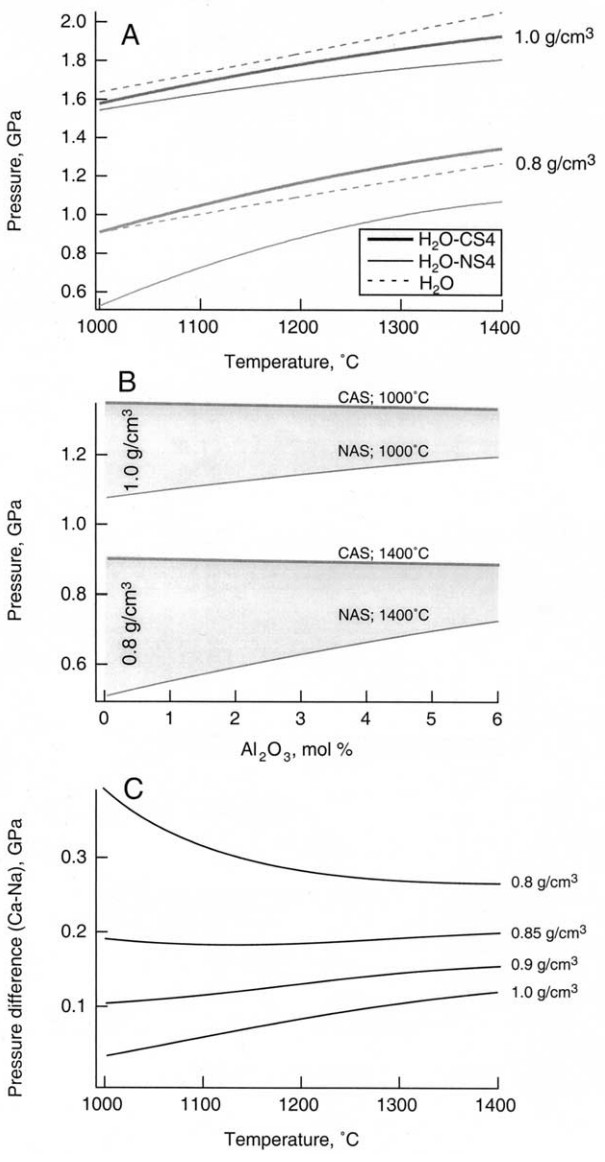

Fig. 13. Isochors for densities indicated in figures for fluids in the systems CaO-Al_2O_3-SiO_2-H_2O (CAS) and Na_2O-Al_2O_3-SiO_2-H_2O (NAS). (A) 1.0 and 0.8 g/cm^3 isochors for Al-free compositions, CS4 and NS4. (B) The effect of Al_2O_3 on the pressure of isochors in CAS and NAS at 1000 and 1400°C. (C) Pressure difference between isochors in the CAS and NAS systems, (Ca-Na) at densities indicated as a function of temperature.

Acknowledgments—This research was conducted with partial support from NSF grants EAR-9901886. A portion of this work was conducted while in residence at the Institut de Physique du Globe de Paris, France. Their hospitality during this stay is greatly appreciated.

Associate editor: C. Romano

REFERENCES

Aoki K. (1987) Japanese island arcs, xenoliths in alkali basalts, high-alumina basalts, and calc-alkaline andesites and dacites. In *Mantle Xenoliths* (ed. P. H. Nixon), pp. 319–333. John Wiley.

Bebout G., Ryan J. G., and Leeman W. P. (1993) B-Be systematics in subduction-related metamorphic rocks: Characterization of the subducted component. *Geochim. Cosmochim. Acta* **57,** 2227–2237.

Bohlen S. R. (1984) Equilibria for precise pressure calibration and a frictionless furnace assembly for the piston-cylinder apparatus. *N. Jb. Mineral. Mh.* **84(9),** 404–412.

Boyd F. R. and England J. L. (1960) Apparatus for phase equilibrium measurements at pressures up to 50 kilobars and temperatures up to 1750°C. *J. Geophys. Res.* **65,** 741–748.

Brodholt J. and Wood B. J. (1993) Simulations of the structure and thermodynamic properties of water at high pressures and temperatures. *J. Geophys. Res.* **98,** 519–536.

Bureau H. and Keppler H. (1999) Complete miscibility between silicate melts and hydrous fluids in the upper mantle: Experimental evidence and geochemical implications. *Earth Planet. Sci. Lett.* **165(2),** 187–196.

Davis N. F. Experimental studies in the system sodium alumina trisilicate-water. Part I. The apparent solubility of albite in supercritical water. *Ph.D. thesis*. 1972 Pennsylvania State University, State College, Pennsylvania.

Eggler D. H. (1972) Water saturated and undersaturated melting relations of a Paricutin andesite and an estimate of water content in natural magma. *Contr. Mineral. Petrol.* **34,** 261–271.

Frantz J. D. and Popp R. K. (1981) The ionization constants of aqueous $MgCl_2$ at elevated temperatures and pressures—a revision. *Geochim. Cosmochim. Acta* **45,** 2511–2512.

Fujii T., Mibe K., and Yasuda A. (1996) Composition of fluid coexisting with olivine and pyroxene at high pressure: The role of water on the differentiation of the mantle. *Seminar on Evolutionary Processes of Earth and Planetary Materials, Misasa, Japan* 37-38. ISEI, Okayama University, Okayama, Japan.

Gaetani G. A., Grove T. L., and Bryan W. B. (1993) The influence of water on the petrogenesis of subduction-related igneous rocks. *Nature* **365,** 332–334.

Gerlach T. M., Westrich H. R., and Symonds R. B. (1996) Pre-eruption vapor in magma of the climactic Mount Pinatubo eruption: Source of the giant stratospheric sulfur dioxide cloud. *Fire and Mud: Eruptions and Lahars of Mount Pinatubo, Philippines* In: (eds. R. S. Punongbayan and C. G. Newhall), p. 415–434. Philippine Institute of Volcanology/University of Washington Press, Washington.

Getting I. C. and Kennedy G. C. (1970) Effect of pressure on the emf of chromel-alumel and platinum-platinum 90 rhodium 10 thermocouples. *J. Appl. Phys.* **11,** 4552–4562.

Haar L, Gallagher J. S., and Kell G. S. (1984) *Steam tables. Thermodynamic and transport properties and computer programs for vapor and liquid states of water in SI units.* Hemisphere Publishing, New York.

Heath E., Macdonald R., Belkin H. E., and Hawkesworth C. F. (1998) Magma genesis at the Soufriere St. Vincent volcano, Lesser Antilles arc. *J. Petrol.* **39,** 1721–1754.

Ionov D. A. and Hofmann A. W. (1995) Nb-Ta-rich mantle amphiboles and micas: Implications for subduction-related metasomatic trace element fractionations. *Earth Planet. Sci. Lett.* **39,** 1721–1754.

Kress V. C. and Carmichael I. S. E. (1991) The compressibility of silicate liquids containing Fe_2O_3 and the effect of composition, temperature, oxygen fugacity and pressure on their redox states. *Contr. Mineral. Petrol.* **108,** 82–92.

Kushiro I. (1972) Effect of water on the composition of magmas formed at high pressures. *J. Petrol.* **13,** 311–334.

Kushiro I. (1976) A new furnace assembly with a small temperature gradient in solid-media, high-pressure apparatus. *Carnegie Instn. Washington Year Book* **75,** 832–833.

Kushiro I. (1990) Partial melting of mantle wedge and evolution of island arc crust. *J. Geophys. Res.* **95,** 15929–15939.

Lange R. A. (1997) A revised model for the density and thermal expansivity of K_2O-Na_2O-CaO-MgO-Al_2O_3-SiO_2 liquids from 700 to 1900 K, extension to crustal magmatic temperatures. *Contrib. Mineral. Petrol.* **130,** 1–11.

Lange R. A. and Carmichael I. S. E. (1987) Densities of Na_2O-K_2O-CaO-MgO-Fe_2O_3-Al_2O_3-TiO_2-SiO_2 liquids: New measurements and derived partial molar properties. *Geochim. Cosmochim. Acta* **51,** 2931–2946.

Manning C. A. (1994) The solubility of quartz in H_2O in the lower crust and upper mantle. *Geochim. Cosmochim. Acta* **58,** 4831–4840.

Mao H. K., Bell P. M., and England J. L. (1971) Tensional errors and drift of the thermocouple electromotive force in the single stage, piston-cylinder apparatus. *Carnegie Instn. Washington Year Book* **70,** 281–287.

Maury R. C., Defant M. J., and Loron J.-L. (1992) Metasomatism of the sub-arc mantle inferred from trace elements in Philippine xenoliths. *Nature* **360,** 661–663.

Merzbacher C. and Eggler D. H. (1984) A magmatic geohygrometer, application to Mount St. Helens and other dacitic magmas. *Geology* **12,** 587–590.

Morey G. W. and Hesselgesser J. M. (1951) The solubility of quartz and some other substances in superheated steam at high pressures. *Am. Soc. Mech. Eng. Trans.* **73,** 865.

Mysen B. O. (1998) Interaction between aqueous fluid and silicate melt in the pressure and temperature regime of the Earth's crust and upper mantle. *N. Nb. Mineral.* **172,** 227–244.

Mysen B. O. and Frantz J. D. (1993) Structure of silicate melts at high temperature, in-situ measurements in the system BaO-SiO_2 to 1669°C. *Am. Mineral.* **78,** 699–1669.

Mysen B. O. and Acton M. (1999) Water in H_2O-saturated magma-fluid systems, solubility behavior in K_2O-Al_2O_3-SiO_2-H_2O to 2.0 GPa and 1300°C. *Geochim. Cosmochim. Acta* **63,** 3799–3816.

Mysen B. O. and Wheeler K. (2000) Alkali aluminosilicate-saturated aqueous fluids in the Earth's upper mantle. *Geochim. Cosmochim. Acta* **64,** 4243–4256.

Mysen B. O. Armstrong L. (2002) Solubility behavior of alkali aluminosilicate components in aqueous fluids and silicate melts at high pressure and temperature. *Geochim. Cosmochim. Acta* (in press).

Mysen B. O. and Wheeler K. (2001) Solubility of Na, Al, and Si in aqueous fluid at 0.8–2.0 GPa and 100–1300°C. In *Water-Rock Interaction* Vol. 10 (ed. R. Cidu), pp. 309–312. A. A. Balkema.

Pitzer K. S. (1983) Dielectric constant of water at very high temperature and pressure. *Proc. Natl. Acad. Sci. USA* **80,** 4575–4576.

Quist S. A. and Marshall W. L. (1968) Electrical conductances of aqueous sodium chloride solutions from 0 to 700°C and pressures to 4,000 bars. *J. Phys. Chem.* **72,** 684–703.

Richet P., Mysen B. O., and Ingrin J. (1998) High-temperature x-ray diffraction and Raman spectroscopy of diopside and pseudowollastonite. *Phys. Chem. Mineral.* **25,** 401–414.

Riter J. C. A. and Smith D. (1996) Xenolith constraints on the thermal history of the mantle beneath the Colorado Plateau. *Geology* **24,** 267–279.

Rutherford M. J. and Devine J. D. (1996) Pre-eruption pressure-temperature conditions and volatiles in the 1991 dacitic magma of Mount Pinatubo. *Fire and mud: Eruptions and lahars of Mount Pinatubo, Philippines* In: (eds. C. G. Newhall and R. S. Punongbayan), p. 751–766. University of Washington Press/Institute of Seismology and Volcanology, Washington.

Sakuyama M. (1979) Lateral variations of H_2O contents in quaternary magmas of Northeastern Japan. *Earth Planet. Sci. Lett.* **43,** 103–111.

Schiano P., Clocchiatti N., Shimizu N., Maury R. C., Jochum K. P., and Hofmann A. W. (1995) Hydrous, silica-rich melts in the sub-arc mantle and their relationship with erupted arc lavas. *Nature* **377,** 595–600.

Shen A. and Keppler H. (1995) Infrared spectroscopy of hydrous silicate melts to 1000°C and 10 kbar, direct observation of H_2O speciation in a diamond cell. *Am. Mineral.* **80,** 1335–1338.

Shibata T. and Nakamura E. (1997) Across-arc variations in isotope and trace element compositions from quaternary basaltic rocks in northeastern Japan: Implications for interactions between subducted oceanic slab and mantle wedge. *J. Geophys. Res.* **102,** 8051–8064.

Skirius C. M., Peterson J. W., and Anderson A. T. (1990) Homogenizing rhyolitic glass inclusions from the Bishop Tuff. *Am. Mineral.* **75,** 1381–1398.

Sobolev A. V. and Chaussidon M. (1996) H_2O concentrations in primary melts from supra-subduction zones and mid-ocean ridges: Implications for H_2O storage and recycling in the mantle. *Earth Planet. Sci. Lett.* **137,** 45–55.

Stalder R., Ulmer P., Thompson A. B., and Gunther D. (1998) Experimental determination of second critical endpoints in fluid/melt systems. *Mineral. Mag.* **62A,** 1441–1442.

Stalder R., Ulmer P., Thompson A. B., and Gunther D. (2000) Experimental approach to constrain second critical endpoints in fluid/silicate systems, near-solidus fluids and melts in the system albite-H_2O. *Am. Mineral.* **85,** 68–77.

Stalder R., Ulmer P., Thompson A. B., and Gunther D. (2001) High pressure fluids in the system $MgO\text{-}SiO_2\text{-}H_2O$ under upper mantle conditions. *Contrib. Mineral. Petrol.* **140,** 607–618.

Swanson S. E., Kay S. M., Brearley M., and Scarfe C. M. (1987) Arc and back-arc xenoliths in Kurile-Kamchatka and western Alaska. In *Mantle Xenoliths* (ed. P. H. Nixon), p. 303–318. John Wiley, New York.

Zhang Y.-G. and Frantz J. D. (2000) Enstatite-forsterite-water equilibria at elevated temperatures and pressures. *Am. Mineral.* **85,** 918–925.

Zotov N. and Keppler H. (2000) In-situ Raman spectra of dissolved silica species in aqueous fluid to 900°C and 14 kbar. *Am. Mineral.* **85,** 600–603.